Orientation and Crystallization of Natural Rubber Network As Revealed by WAXD Using Synchrotron Radiation

Masatoshi Tosaka,* Syozo Murakami, Sirilux Poompradub, and Shinzo Kohjiya

Institute for Chemical Research, Kyoto University, Uji, Kyoto 611-0011, Japan

Yuko Ikeda

Kyoto Institute of Technology, Matsugasaki, Kyoto 606-8585, Japan

Shigeyuki Toki, Igors Sics, and Benjamin S. Hsiao

Department of Chemistry, State University of New York at Stony Brook, New York 11794-3400

Received October 16, 2003; Revised Manuscript Received February 17, 2004

ABSTRACT: Strain-induced crystallization of natural rubber samples with various network-chain densities, ν, was investigated by synchrotron X-ray diffraction measurements. It was found that the onset strain of crystallization was almost independent of ν. Lateral crystallite size and degree of orientational fluctuations of crystallites were also evaluated. These results indicated that stretched molecular chains acted as nuclei while surrounding chains could also contribute to the crystal growth. Deformation of crystal lattice with nominal stress was detected, and the strain-induced crystallites were found to be responsible for the increased modulus upon elongation. The unit cell volume decreased almost linearly with nominal stress. By assuming the deformation mechanism of the rubber network as a pantograph, the reinforcement effect of the crystallites is thought to be brought out not directly by crystallites connected in series but indirectly through the surrounding network chains.

Introduction

Strain-induced crystallization of natural rubber (NR) has been extensively studied even before the advent of macromolecular physics.[1] However, there are still some unsolved issues in this field. For example, the fundamental molecular mechanism of strain-induced crystallization in cross-linked rubber is still unclear. Flory[2] proposed a thermodynamic theory for strain-induced crystallization of network polymers, in which the growth of crystallites in the direction parallel to the chain (orientation) axis was implicitly assumed. Another school of theory, led by a German research group,[3,4] assumed the development of lamellar crystallites, meaning that the crystallites grow in the direction perpendicular to the molecular chain axis. Though morphological studies based on electron microscopy of un-cross-linked NR revealed the growth of lamellar crystals,[5−9] another study reported that the evidence of the lamellar crystals disappeared by increasing the cross-linking density.[10] To the authors' knowledge, no conclusive evidence has ever been presented with respect to the crystal growth direction in NR with different cross-linking density.

Another unresolved issue is the role of strain-induced crystallites on the mechanical response of NR. Because crystallization is always accompanied by a considerable increase in modulus, the strain-induced crystallites have been thought to bear the tensile stress. However, the possibility that the increased modulus is due to the limited extensibility of the network chains still remains. In other words, apportioning of the applied stress to the crystalline and amorphous components should be considered. For such crystallization studies, wide-angle X-ray diffraction (WAXD) measurements have been effective to study development of crystalline structures induced by deformation. For example, Mitchell[11] estimated the orientation parameter and crystallinity from the WAXD data and reported their changes with strain. He noticed that the amorphous component has only a small degree of preferred orientation. Consequently, the crystallinity was calculated from the fraction of decreased amorphous component, which was estimated by the decrease in the intensity of the amorphous halo measured at a fixed position on the equator. This method gives approximate values for crystallinity, but the reliability of the estimated values decreases when the degree of localization of amorphous halo intensity increases. In our previous publications,[12,13] tensile and simultaneous WAXD measurements were performed by using a powerful synchrotron X-ray source. The WAXD patterns were deconvoluted into three components: crystalline, oriented amorphous, and isotropic phases. On the basis of this analysis, we have reported the development of crystalline and oriented amorphous fractions with strain. At the same time, the existence of a significant amount of isotropic amorphous component even in highly stretched NR vulcanizate was also identified. According to these results, the load on the rubber sample should be borne only by a minor fraction of crystalline and oriented amorphous components.

In this study, the strain-induced crystallization of vulcanized NR with different cross-linking density was investigated by using simultaneous synchrotron X-ray diffraction and tensile measurements. This dynamical study enabled us to collect WAXD patterns before significant relaxation of the sample and to follow the structural development in real time. Our goal in this study is to understand the effect of cross-linking density or network-chain length on strain-induced crystalliza-

* Corresponding author: Tel +81-774-38-3062; Fax +81-774-38-3067; e-mail tosaka@scl.kyoto-u.ac.jp.

10.1021/ma0355608 CCC: $27.50
Published on Web 04/07/2004

Table 1. Specification of Vulcanized NR Samples

sample code	NR-1	NR-2	NR-3	NR-4	NR-5
rubber,[a] phr[b]	100	100	100	100	100
stearic acid, phr[b]	2	2	2	2	2
active ZnO, phr[b]	1	1	1	1	1
CBS,[c] phr[b]	3	2	1.5	1	0.75
sulfur, phr[b]	4.5	3	2.25	1.5	1.125
total, phr[b]	110.5	108	106.75	105.5	104.875
curing time,[d] min	10	12	12	14	18
network-chain density $\times 10^4$, mol/cm^3	2.12	1.78	1.46	1.31	1.01

[a] RSS no. 1 from Malaysia. [b] Parts by weight for hundred parts of rubber. [c] *N*-Cyclohexyl-2-benzothiazole sulfenamide. [d] Cure temperature was 140 °C.

tion in rubber. In particular, we wish to present an exact molecular mechanism concerning the strain-induced crystallization in cross-linked materials.

Experimental Section

Vulcanized NR (RSS no. 1) samples were prepared according to the recipes and cure conditions outlined in Table 1. The cure temperature was 140 °C for all the samples. In advance of the curing process, each cure time was determined on the basis of the result of cure characteristics from a JSR Curelastmeter III, which was used to monitor the progress of curing. Network chain density (ν) values of the samples were estimated according to eq 1 based on the classical theory of rubber elasticity.[14]

$$\sigma = \nu kT(\alpha - \alpha^{-2}) \quad (1)$$

where σ is the force per unit area, ν is the number of network chains in unit volume, k is the Boltzmann constant, T is the absolute temperature, and α is the elongation ratio ($\alpha = l/l_0$, in which l_0 is the initial length of the sample and l is that of the elongated sample). A plot of σ vs ($\alpha - \alpha^{-2}$) gives a straight line in accord with eq 1, and the value of ν is calculated from the initial slope. The estimated ν values are included in Table 1. Each rubber compound was molded into a sheet of 1 mm thickness by heat-pressing using a mold. The specimens for simultaneous synchrotron X-ray and tensile measurements were cut out from the sheet into a dumbbell shape. The initial width and thickness of the parallel part of the specimen that was exposed to the X-ray were 3 mm and 1 mm, respectively.

The original stretching machine has been described in our previous papers.[15−17] This apparatus was modified for higher elongations[12] and was used in this study. The specimen was stretched horizontally in a symmetric fashion so that the X-ray irradiated almost the same position of the specimen. The distance between the clamps was 24 mm, and the deformation rate was 10 mm/min. The tensile stress applied to the sample was recorded as a function of elapsed time. To determine the exact strain values, the deformation of the specimen was photographed periodically. The initial samples were marked beforehand, and the changing distance between the marks was determined from the photographs. From the mark-to-mark distance, the strain value was calculated as a function of elapsed time.

The synchrotron X-ray measurements were carried out at the X27C beamline in the National Synchrotron Light Source, Brookhaven National Laboratory. The wavelength was 0.1366 nm. The two-dimensional WAXD patterns were recorded using a MAR CCD camera. Exposure time for each image was 30 s, and there was an interval of 5 s before the next exposure. The sample was continuously deformed during the exposure. The diffraction angle was calibrated by an Al_2O_3 standard (provided by the National Institute of Standards and Technology). The images were processed using software named "POLAR" (Stonybrook Technology and Applied Research, Inc.).

Results

Stress−Strain Behavior. An example of the stress−strain curve of the NR sample is shown in Figure 1. As

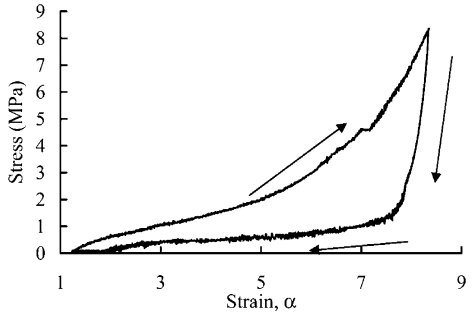

Figure 1. Stress−strain curve of NR-4. α is the elongation ratio defined as $\alpha = l/l_0$, in which l_0 is the initial length of the sample and l is that of the elongated one. Arrows indicate the direction of deformation.

shown before, the sample with the larger ν showed the higher modulus in the tensile measurements of this study. In Figure 1, a noticeable upturn in stress was observed in the stretching process after α exceeded ca. 4. When the retracting process started, the stress decreased abruptly. In this study, all samples were stretched at the same deformation rate and with the same clamp-to-clamp initial length. However, the maximum strain values at the measured part of the dumbbell-shaped specimens were different from sample to sample. This is partly due to the slipping of the sample from the clamps and partly due to inhomogeneous deformation of the dumbbell-shaped specimen.

Fraction of Crystalline Component. Figure 2 shows typical changes in WAXD patterns from an NR sample during the stretching (Figure 2a−d) and retracting (Figure 2d−g) processes. At small strains during stretching, highly oriented reflections of fatty acids[18] were recognized on both sides of the beamstop (Figure 2b,h, indicated by arrows). Crystalline reflections of NR appeared afterward. It is interesting to note that even at the onset of crystallization, the NR crystallites were highly oriented (Figure 2c). A strong isotropic amorphous halo persisted[12,13] even at 800% (the maximum strain), as shown in Figure 2d. In the retracting process, the crystalline reflections disappeared gradually. Some crystalline reflections remained at smaller strains, during retraction, which can be recognized by comparison of parts b and f of Figure 2. When the sample was totally relaxed, the isotropic amorphous halo returned to the original shape (Figure 2g). Ringlike (unoriented) crystalline reflections of NR were not observed during the cyclic deformation process.

In our previous papers,[12,13] the WAXD pattern was regarded to be composed of isotropic, oriented amorphous, and crystalline components and was deconvoluted into three corresponding patterns. In this paper, we deconvoluted the WAXD pattern in a similar way. After subtraction of the air scattering from the starting WAXD pattern, the isotropic amorphous component was extracted, representing the WAXD pattern for the unstretched sample. The remaining of the pattern, containing the oriented amorphous and crystalline components, was azimuthally integrated in the range of ±75° from the equator to give a radial intensity distribution. The reason for limiting the angular range for integration was that the reflections near the meridian could not satisfy the undistorted reflection condition in an oriented specimen.[19] The radial intensity distribution integrated as above, with range corresponding to 0.25−1 nm in real space, was decomposed by 1-dimensional peak fitting into several peaks, each representing

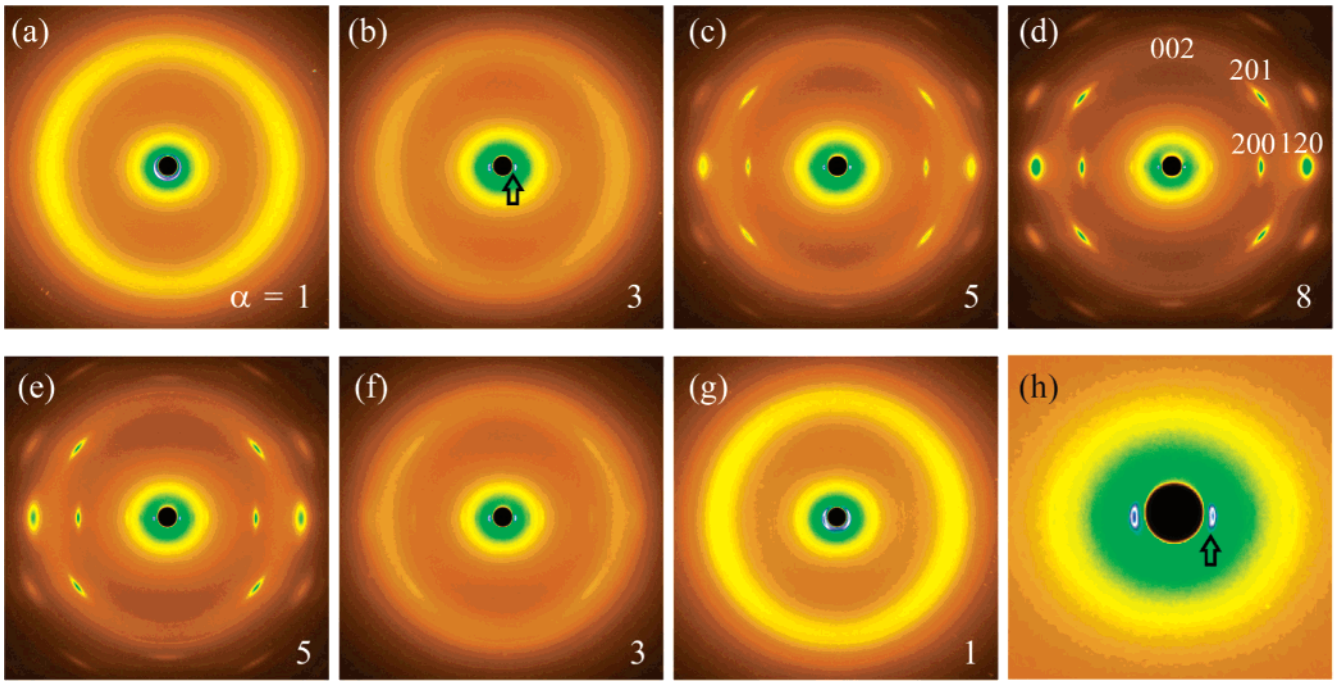

Figure 2. Sequential change of WAXD patterns from NR-4. Stretching direction is vertical. Corresponding strain values are indicated at the right bottom in parts a−g of the figure. Indices of crystalline reflections of NR are indicated in part d. Part h shows the enlarged image of the center of part b. Sharp reflections from fatty acids (indicated by arrows) corresponding to ca. 4.2 nm in real space are recognized on both sides of the beamstop.

oriented amorphous and crystalline components, as in our previous papers.[12,13] Then, the intensity of each (crystalline or oriented amorphous) peak was converted into a corrected value considering the geometrical factor of the experiment and the symmetry of the sample. The corrected intensities were used to estimate the "crystallinity index" (CI). The calculation of CI from the results of peak fitting is described as follows:

$$\mathrm{CI} = \frac{\sum_{\text{crystal}} 2\pi \int \sin\phi \, \mathrm{d}\phi \int I(s)s^2 \, \mathrm{d}s}{\sum_{\text{total}} 2\pi \int \sin\phi \, \mathrm{d}\phi \int I(s)s^2 \, \mathrm{d}s} \qquad (2)$$

In eq 2, $I(s)$ represents the intensity distribution of each peak that is read out from the WAXD pattern, s is the radial coordinate in reciprocal space in nm^{-1} unit ($s = 2 (\sin \theta)/\lambda$, where λ is the wavelength and 2θ is the scattering angle), and ϕ is the angle between the scattering vector of the peak and the fiber direction. The integral covers the range of a peak in question, and the summation is calculated for each peak. The numerator and the denominator are related to the amount of crystalline and total components, respectively. CI values should give estimates close to the real volume fractions,[20] even with considerable localization of the amorphous halo intensity.

Figure 3a−e shows the hysteresis curves of CI for the samples with different cross-linking densities. All the curves for CI showed similar trends. The crystallization started after the sample was elongated to some extent. In the retracting process, CI possessed a higher value than that in the stretching process, and its value remained nonzero even at small strain values where no crystalline reflection was detected.

In Figure 4, the CI values during the stretching process are plotted together for all samples. It was interesting to find that the onset strain of crystallization (α_c) was almost independent of ν. This point was further confirmed by the inspection of the original X-ray patterns; in all samples, crystalline reflections started to appear at a strain value of ca. 3.2. The sample with the larger ν typically exhibited a steeper slope in the plot.

Lateral Crystallite Size. To evaluate the variations of crystallite size, the widths of the 200 and 120 reflections were estimated. The intensity distribution on the equator was extracted from the original WAXD pattern, and each peak was fitted with a linear background and a Gaussian function having the form

$$I(x) = h \exp[-(x - x_c)^2/(2w^2)] \qquad (3)$$

where $I(x)$ is the intensity at position x, x_c is the position at the scattering maximum, and h and w are parameters related to the peak height and the peak width, respectively. Each of w value was converted into the half-width β. (The conversion procedure is described in Appendix 1.) The crystallite size was estimated by using the Scherrer equation

$$L_{hkl} = K\lambda/(\beta \cos \theta) \qquad (4)$$

where L_{hkl} is the crystallite size in the direction perpendicular to the (hkl) plane, λ is the wavelength, and θ is the Bragg angle (half of the scattering angle). In this study, the value 0.89 was tentatively used for K.[21]

Figure 5 shows the variations of the crystallite size estimated from the 200 and 120 reflections (see Appendix 2). Both L_{200} and L_{120} showed a similar trend. During the stretching process, the crystallite size decreased continuously with strain for all samples. The sample with the larger ν showed the smaller crystallite size. When the samples were allowed to retract, the crystallite size increased first and then decreased due to crystal melting.

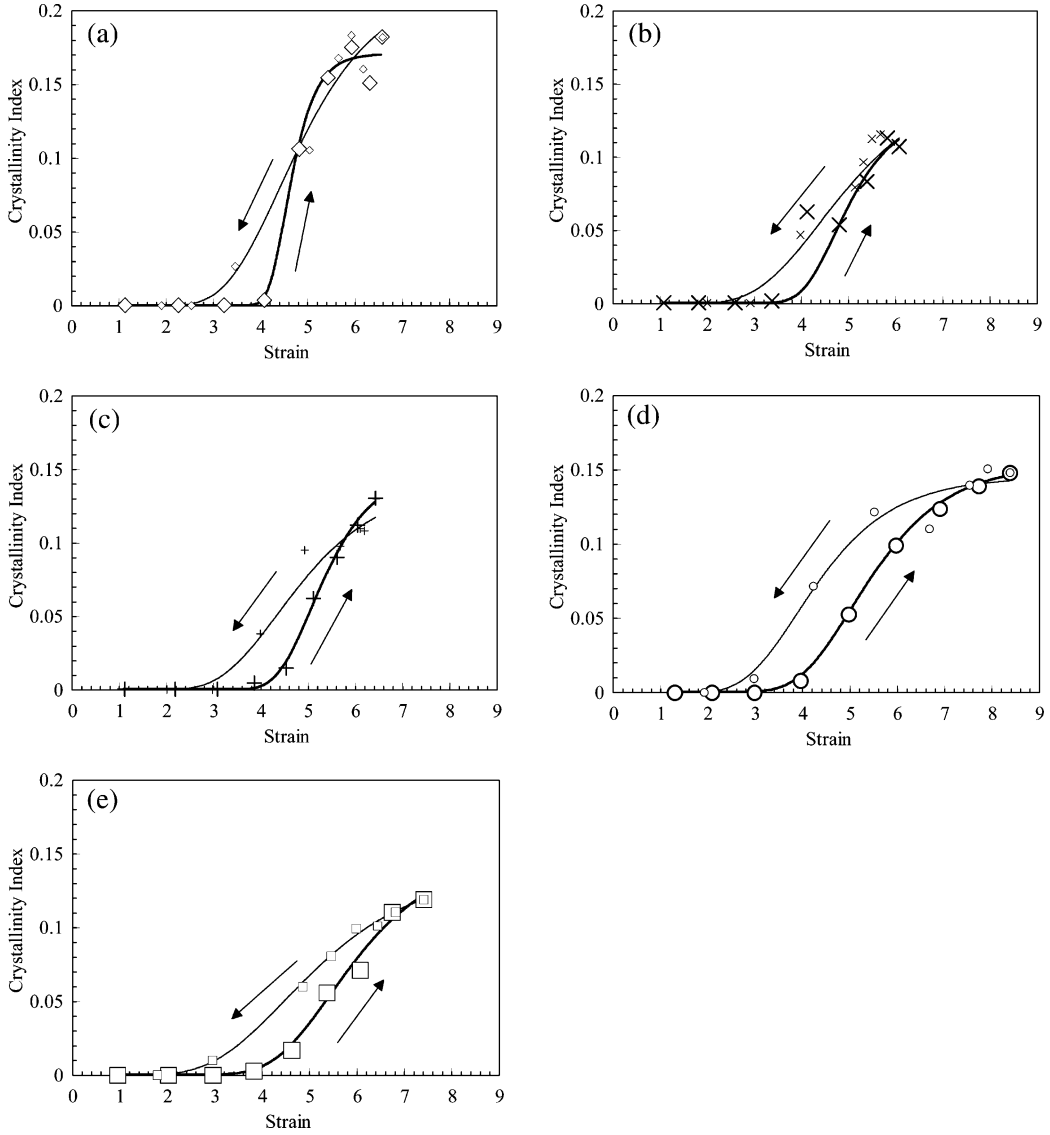

Figure 3. Variation of CI values with strain for NR samples: (a) NR-1, (b) NR-2, (c) NR-3, (d) NR-4, (e) NR-5. Thick lines and larger symbols indicate the stretching process, and thin lines and smaller symbols the retracting process.

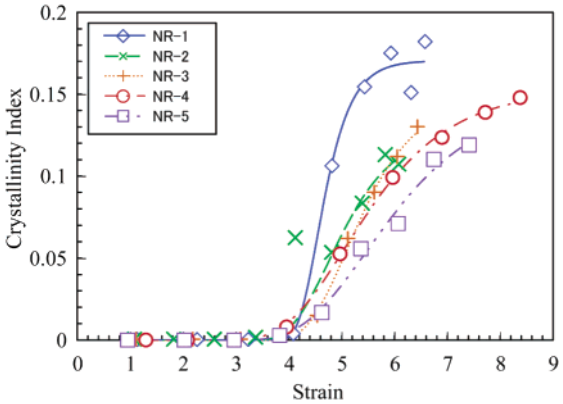

Figure 4. Comparison of crystallization behavior during the stretching process for samples with different network-chain densities.

Orientational Fluctuations of Crystallites. The degree of orientational fluctuations of crystallites was evaluated from the intensity distribution of the 200 reflection, which was obtained by the azimuthal scan of the peak. In a similar procedure as outlined earlier, the width parameter in the azimuthal direction, w_{az}, was obtained by fitting the intensity distribution with a Gaussian function (eq 3). Then w_{az} was converted into half-width β_{az} (see Appendix 1, eq A4). The smaller value of β_{az} indicates the smaller fluctuations in orientation. Results are shown in Figure 6. Just after the formation of crystallites, β_{az} became smaller, indicating an improved degree of orientation. Upon further elongation, β_{az} fluctuated little, but the value seemed to remain about constant. In this case, the sample with the larger ν showed a smaller β_{az}, i.e., a smaller orientational fluctuations of crystallites. When the retraction process started, β_{az} of all samples first became smaller and then increased due to crystal melting and relaxation of the system.

Deformation of the Crystal Lattice with Nominal Stress. To evaluate the deformation of the crystal lattice, the lattice constants were estimated from each WAXD pattern during the deformation process by using the least-squares regression method. The rectangular unit cell proposed by Nyburg[22] was assumed. Estimated values of the lattice constants and the volume of the unit cell are plotted against stress in Figure 7. Despite the scatter of the values, there are noticeable apparent systematic variations. The unit cell contracts along the

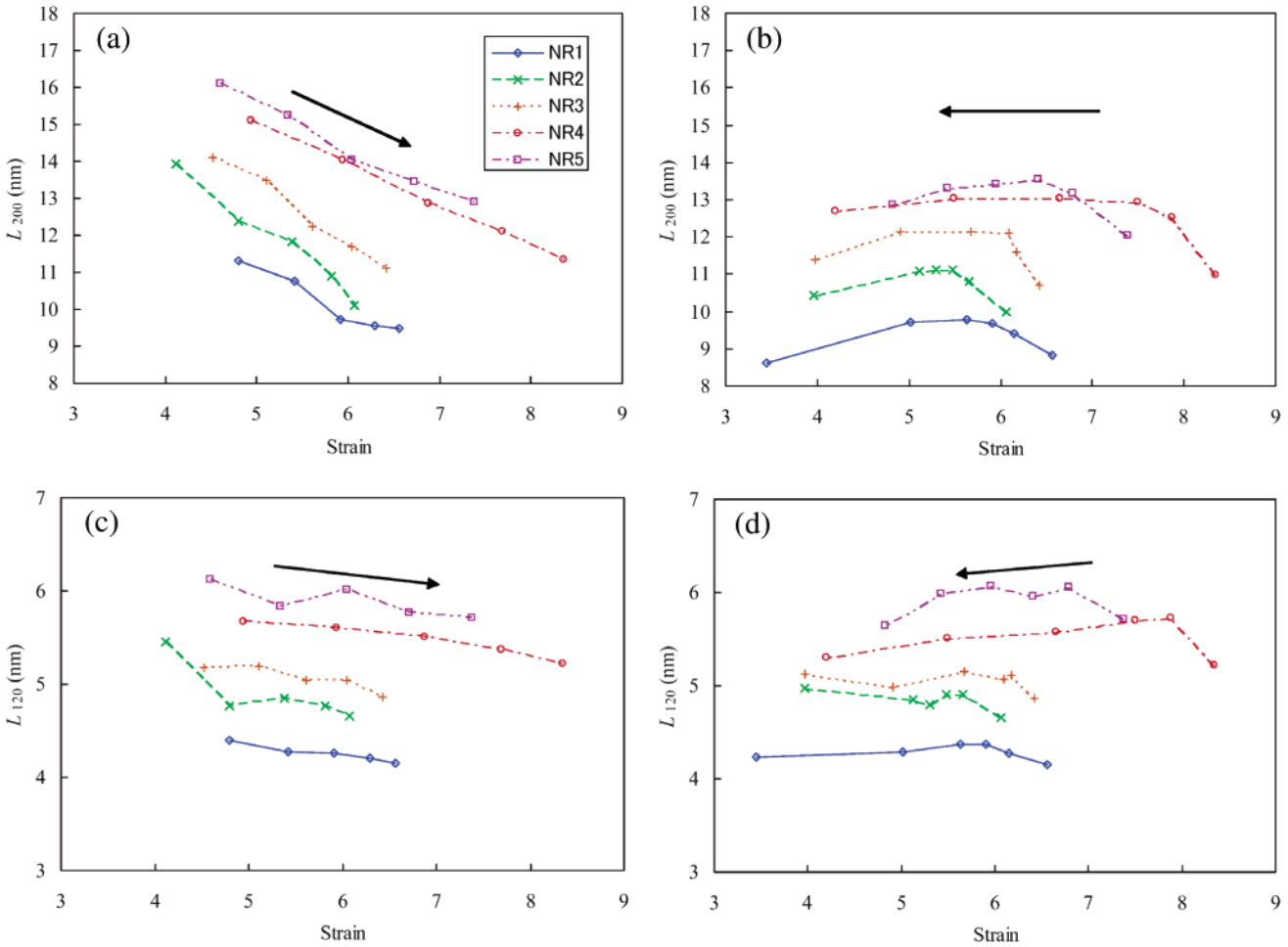

Figure 5. Variation of lateral crystallite size as defined in eq 4 with strain: (a) L_{200} during the stretching process, (b) L_{200} during the retracting process, (c) L_{120} during the stretching process, and (d) L_{120} during the retracting process.

a- and *b*-directions (perpendicular to the stretching direction) and elongates in the *c*-direction (parallel to the stretching direction). If the systematic variation of the lattice constants were due to a small shift of the camera length during the deformation process, then all parameters in the three directions would increase, or all of them would decrease, which was not seen in this study. The existence of simultaneous increase and decrease in the same set of lattice parameters indicates that they were changed by deformation. The volume of the unit cell was found to decrease with the increase in the nominal stress. It was interesting to observe such a volume change because the Poisson's ratio of rubber is usually assumed to be 0.5, meaning no volume change upon deformation. However, this is valid only if rubber is liquidlike amorphous and incompressible. In the case of WAXD measurements, the crystalline part of NR is in the ordered solid state, and thus the volume change is possible due to better ordering of the chains. The degree of deformation of the unit cell exhibited an almost linear relationship with the nominal stress. This implied that the crystal lattice was deformed elastically by the nominal stress. The deformation of the crystal lattice is a direct evidence indicating that the strain-induced crystallites are responsible for the load increase and hence the increase in the modulus of NR upon stretching. The values of the lattice constants at zero stress, which can be estimated from the extrapolation of the plots in Figure 7, were larger than those reported by former researchers (for example, $a = 1.246$, $b = 0.889$, $c = 0.81$ nm).[22] This difference may be due to the difference in the experimental temperature. For example, the reported unit cell constants by Nyburg[22] were obtained from the sample maintained at −25 °C, while we obtained the values from the sample at room temperature. Because of the thermal expansion of the crystal lattice, we have obtained the larger values of the lattice parameters.

Discussion

Molecular Mechanism of Deformation before the Onset of Crystallization. On the basis of the above results and previous observations, the process of strain-induced crystallization in cross-linked rubber is discussed here. At first, attention is paid to the period before the emergence of rubber crystals (that is, during the stretching process, $\alpha < 3$). It has been well documented that when the elongation of the sample is started, immediate development of birefringence is usually seen.[23−25] We have also observed the highly oriented reflections of fatty acid crystals at a small angle region on the equator before the emergence of crystalline reflections of NR (Figure 2b,h). These results indicate that the rubber sample was oriented and molecular anisotropy was developed. However, the amorphous halo was largely isotropic during this period, and only a small degree of localization in intensity was recognized in the WAXD pattern (Figure 2b). To explain these paradoxical observations, we must consider all the dimensions that were detected by the experimental methods. Orientation

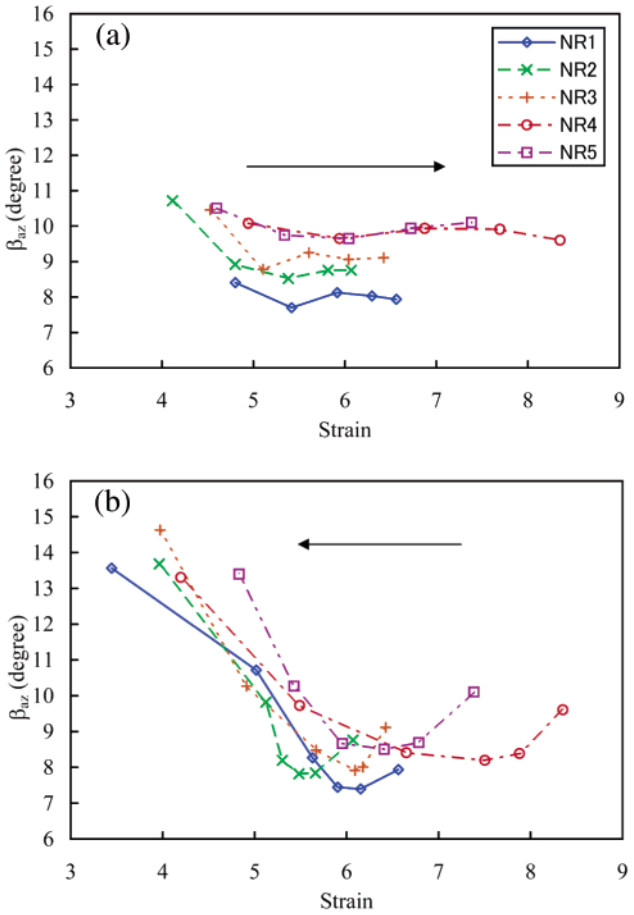

Figure 6. Variation of the azimuthal half-width of the 200 reflection β_{az} with strain during (a) the stretching process and (b) the retracting process.

of fatty acid crystals (flake-shaped[18]) may reflect structures greater than 10 nm in NR. On the other hand, the amorphous halo in the WAXD patterns reflects the structure with dimensions below 1 nm. A possible explanation for the current observation is that some structures of the larger scale are oriented (which may also be responsible for the development of birefringence), while those of the smaller scale are almost isotropic. Such a scenario can be achieved if the system is, for example, deformed like a pantograph, as illustrated in Figure 8. In this figure, the end-to-end vector (drawn with a thick blue line in Figure 8) of a network chain is regarded as the frame of the pantograph. In the undeformed state, each network chain is randomly coiled, forming a globule; thus, the end-to-end vector is randomly oriented (Figure 8a). When the sample is stretched at a small strain, the average size of the end-to-end vectors is changed only slightly, while the directors would be rotated and the globules would be rearranged to accommodate the macroscopic elongation, as if a pantograph expands in the diagonal direction. It is conceivable that many globules can still remain in the original undeformed state (Figure 8b) during this deformation stage, which will result in the isotropic amorphous halo in the X-ray diffraction patterns. Elongation of a small fraction of relatively short network chains may be required to enable such a deformation mechanism.

Onset of Crystallization. Further elongation of the NR samples induces a distinct crystallization process. The schematic model of deformation of network chains is illustrated in Figure 9. Because the crystalline reflections are highly oriented from the emergence, the crystallites must have been initiated from oriented nuclei. The nuclei may consist of single or assemblies of network chains that are highly oriented by stretching. Formation of one kind of such nuclei from single chain stems is illustrated in Figure 9a,b. The molecular chains contributing to the crystal growth may be supplied from the surrounding coiled chains, resulting in lateral crystal growth as shown in Figure 9c. Because the growth of lamellar crystals is reported in both un-cross-linked[5−9] and lightly cross-linked[10] NR, this model of crystal growth should be reasonable. There may be another model of crystal growth that the sporadically occurred stretched chains are bundled and form fibrillar crystallites with fringed micelle structure. The latter model should lead to a larger crystallite size for the sample with larger ν. However, the results in Figure 5 show an opposite trend.

The onset of crystallization could be determined by the increase in melting temperature due to the strain. A simple explanation for this argument has been made by Yamamoto and White,[26] which is described as follows. The melting temperature $T_{m,1}$ in the undeformed state can be given as

$$T_{m,1} = \Delta H_1/\Delta S_1 \tag{5}$$

When the sample is deformed, the melting temperature will be increased by an amount

$$T_{m,\alpha} - T_{m,1} = (\Delta H_\alpha/\Delta S_\alpha) - (\Delta H_1/\Delta S_1) \tag{6}$$

If the heat of fusion is independent of deformation, then the above equation becomes

$$1/T_{m,\alpha} = (1/T_{m,1}) - (\Delta S_{def}/\Delta H_1) \tag{7}$$

In the above equations, ΔH is the heat of fusion, ΔS is the entropy of fusion, the subscripts α and 1 indicate the strain values, and ΔS_{def} is the difference of the entropy between the undeformed and the deformed states. Equation 7 indicates that melting temperature increases with strain because ΔS_{def} is a function of strain. Thus, as $T_{m,\alpha}$ becomes higher than room temperature, the system comes into a supercooled state. Because the nuclei (namely stretched network chains that were described in the previous section) are present and thermally stable, the crystallization can start immediately as the large supercooling becomes a strong driving force for crystallization. The origin of ΔS_{def} may be partly due to the orientation and/or deformation of the end-to-end vector of the network chains. The affine-like deformation of globular coils (red ellipsoids in Figure 8b) can also be considered when the elongation ratio is high. However, crystallization will convert the elongated coil into a combination of a fully stretched crystalline chain portion and an unstretched amorphous chain portion in the random-coil-like state, as explained below.

Flory[2] has commented that "the entropy of the amorphous portion generally is increased by crystallization" because the chains in the crystallites are stretched, and "this change permits the amorphous portion of the chain to assume a greater number of configurations". In this way, the strain of the chains in the amorphous portion is far below the macroscopic strain, as has been pointed out by other researchers.[3,4,14]

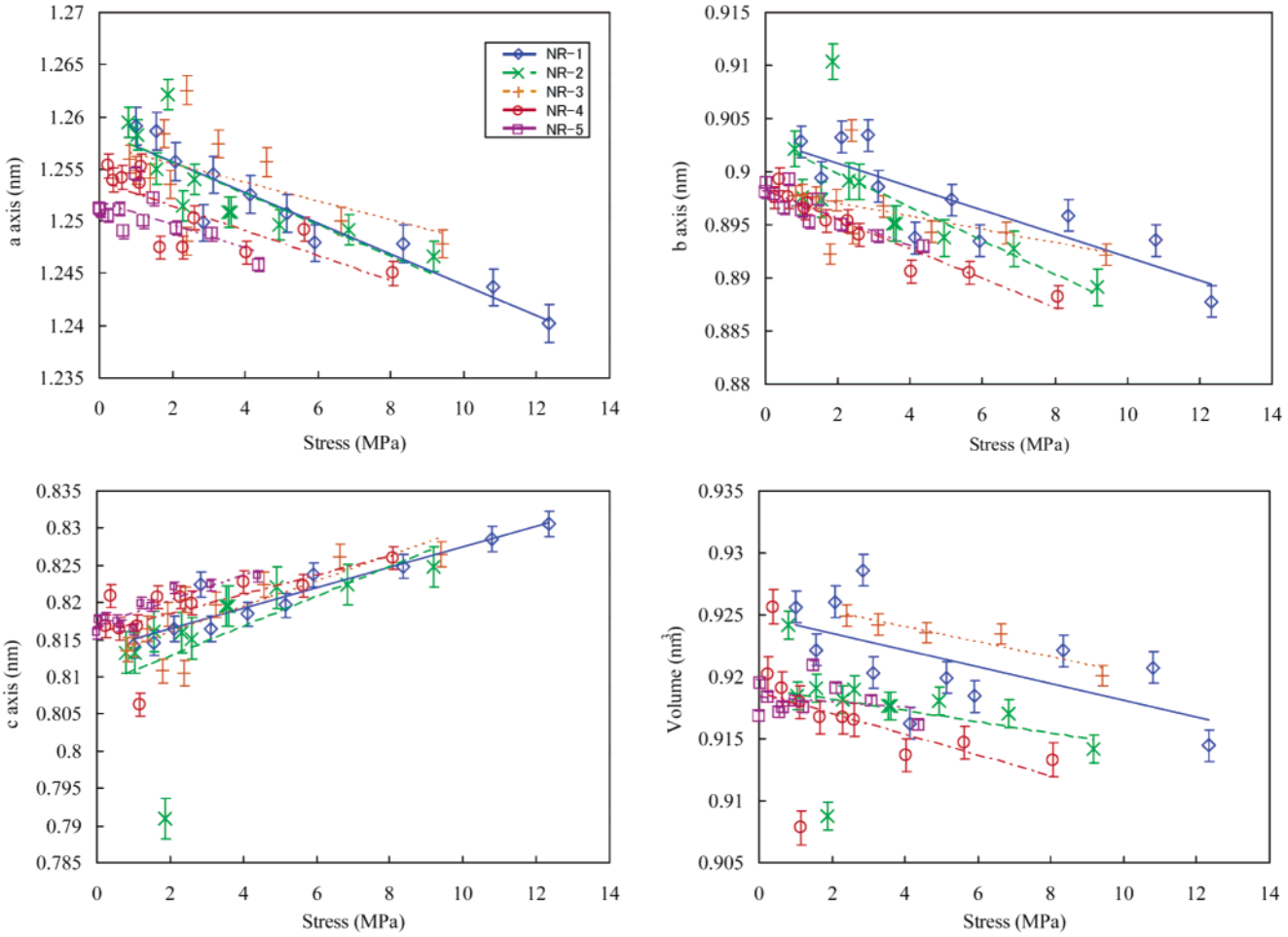

Figure 7. Deformation of the crystal lattice with nominal stress. The vertical bars indicate standard errors. The straight lines are drawn based on the regression analysis.

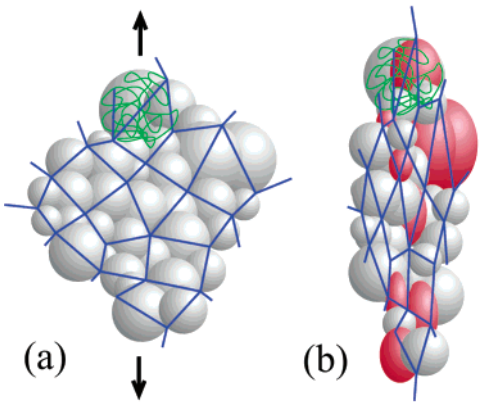

Figure 8. Schematic representation of deformation like a pantograph. Spheres indicate globules of coiled network chains. Thick lines indicate end-to-end direction of the network chains. The coiled molecular chain is drawn in green only in a globule at the top of the figure. (a) Before deformation, all globules have spherical shape. (b) Even after deformation, only a part of the globules is elongated, which are drawn in red.

This is not only a theoretical assumption but there are also experimental evidences, for example: (1) in the case of synthetic *cis*-1,4-polyisoprene (the main constituent of NR), a decrease in nominal stress due to crystallization has been observed,[27] indicating that the rubber molecules are elongated in the crystallites and the remaining amorphous portion is relaxed; (2) orientational functions of cross-linked NR molecular chains were estimated separately for crystalline and amorphous components by measuring infrared dichroism, and a slight decrease in the orientational function of the amorphous component was observed at the onset of strain-induced crystallization, indicating the slight disorientation of the polymer segments in the amorphous phase due to the crystallization.[28] These discussions are applicable to the current case. In the stretched and crystallized NR samples, the chains in the amorphous portion may be in a random-coil-like state. This is a possible explanation why the halo of isotropic amorphous was consistently observed even from the highly stretched sample. On the basis of this idea, development of crystallization will reduce ΔS_α, and hence the degree of supercooling, of the surrounding amorphous portion. At the same time, the latent heat exposed by crystallization will also play a role to reduce the supercooling. As a result, strain-induced crystallization will be hindered by the actual event of crystallization itself. This idea is consistent with our observation. It is thought that the crystallite size would be independent of ν before the growing crystallites collide with each other, if the crystal growth is not hindered by any other factors. However, in this study, we observed that the crystallite size of the sample with the larger ν was smaller (Figure 5) even when crystallinity was very low (just after the onset of crystallization). This can be explained as follows: When a certain amount of crystallites is formed, the resultant increase in entropy in the amorphous portion will hinder further crystallization. In the sample with the larger ν, the number of

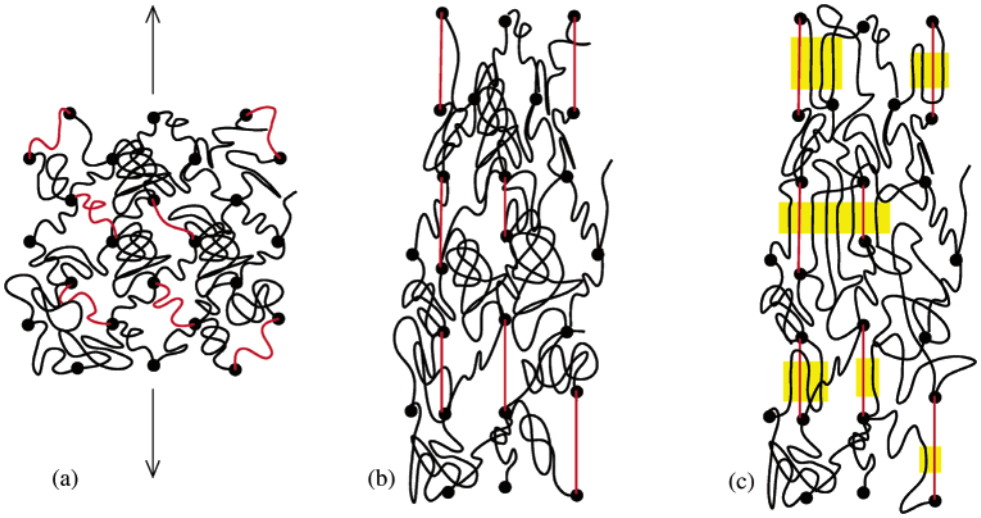

Figure 9. Model of nucleation and crystallization in vulcanized NR. Relatively short chains are drawn as red lines. Filled circles represent cross-links. (a) Before deformation: cross-links are distributed uniformly for easier understanding. (b) After deformation: short chains are fully stretched. Note that the distribution of cross-links is no longer uniform to keep many network chains in the random-coil-like state. (c) The fully stretched chains act as nucleus of crystallites (yellow parts).

nuclei, and hence the number of crystallites, is larger. Therefore, the amount of crystallites becomes sufficient to stop further growth even when the crystallites were smaller.

Development of Crystallites. With the macroscopic elongation of the sample, the number of stretched chains that can act as nuclei must increase. As a result, the mean distance between the nuclei must decrease and the average crystallite size should also become smaller. Because of the same reason, as mentioned above, the larger ν value should have resulted in the smaller crystallite size. We believe that the orientational fluctuations of the crystallites are related to the crystallite size. In Figure 6, it was found that the higher the ν value, the smaller fluctuations of the crystallites (β_{az}). There are two possible reasons for the orientational fluctuations: (1) one is due to the fluctuations of the oriented nuclei, and (2) the other is development of the fluctuations during the crystal growth. It is very difficult to explain the former, that is, the dependence of orientational fluctuations of the nuclei on ν, because only the size of the network should be different between the samples of different ν; the director of the network chain must be independent of ν. Concerning the latter, bending of lamellar crystal has been reported for many polymer species and has also been related to the undulation of chain axis in the crystallites.[29,30] Because of the bending of lamellar crystals, the larger crystallites in the sample with the smaller ν may have a higher degree of orientational fluctuations as shown in Figure 10. Figure 10a illustrates a crystallite grown from a nucleus that is represented by thick vertical lines in the center. The molecular stems in the neighborhood of the nucleus align almost parallel to it. However, those located far from the nucleus tend to depart from the parallel alignment because of the bending of the lamella, as represented by the thick red lines on the both edge of the crystallite. Figure 10b illustrates the case of small crystallites grown from a dense distribution of nuclei that are represented by thick vertical lines in the center of each crystallite. The orientation of nuclei is assumed to be almost parallel to each other. Because of the smaller crystallite size, the molecular stems in the crystallites are all located in the neighborhood of the nuclei, and accordingly, most of the stems align almost parallel to the nuclei. Because the bending of lamellae has been related to the chain folding, our results implicitly indicate the existence of chain folding on the surface of crystallites in cross-linked NR. Since β_{az} in Figure 6 is almost constant for each sample, and the decrease in crystallite size with strain is also seen in Figure 5, we can raise the following question. If β_{az} is related to the crystallite size, why was the change of β_{az} with strain, and hence crystallite size, not observed? It is conceivable that the director of the stretched chains, namely the nuclei, has been perturbed due to the induced crystallites after the onset of crystallization, and the depression of β_{az} due to the decrease of crystallite size has been compensated by the perturbation. The slight change in β_{az} with strain (Figure 6) may have reflected the balance of the opposite effects.

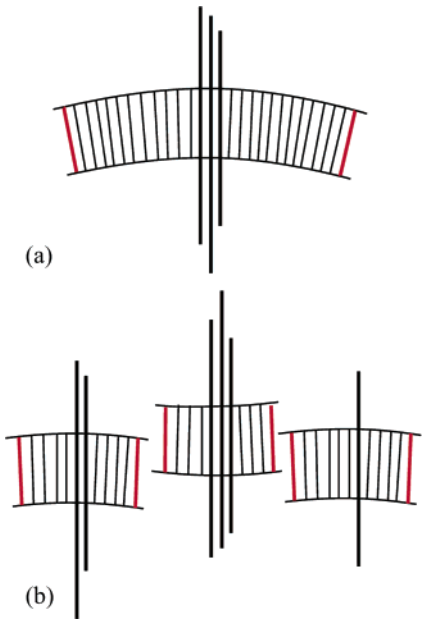

Figure 10. Orientational fluctuations of crystallites due to bending of lamellae. Thick lines in the center of each crystallite represent nuclei. Directions of thick red lines on both sides of crystallites should be compared. Degree of fluctuations in the larger crystallite in (a) is larger than that in smaller crystallites in (b).

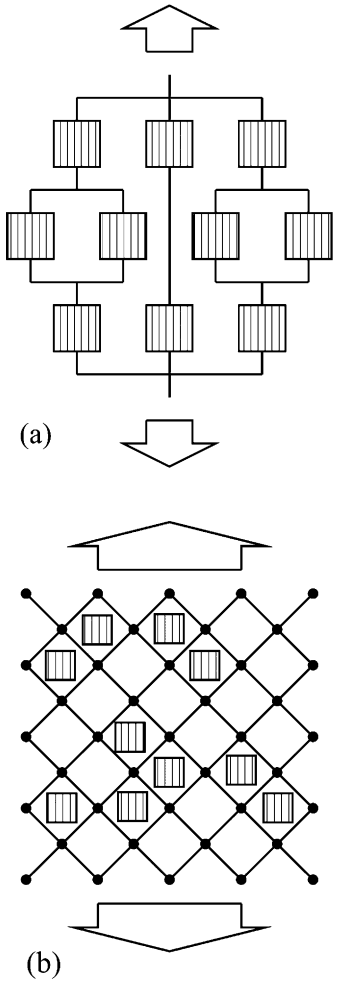

Figure 11. Mechanical models to explain the deformation of crystallites. Filled squares indicate crystallites. (a) Combination of serial and parallel connections of crystallites. (b) Crystallites are located between the frames of surrounding chains that transmit the nominal stress to the crystallites by the deformation as a pantograph.

Stress on Crystallites. As has been described earlier, the unit cell of the NR crystallites is elongated along the *c*-direction while it shrinks along the *a*- and *b*-directions. There are two pathways to deform the crystallites in such a manner; one is to stretch the crystallites along the stretching (*c*-) direction, and the other is to compress them perpendicularly to the stretching direction.

As the mechanical model to explain the deformation of the rubber crystallites, one may first imagine the combination of serial and parallel connections of crystallites pulled in the stretching direction, as shown in Figure 11a. (It is not possible to fill the 3-dimensional space only by one type of serial or parallel connections. In this figure, the compression in the horizontal direction is unexpected.) However, such a model is inconsistent with the linearity of the lattice deformation with the nominal stress (Figure 7) because of the following reason. During the deformation process, both the nominal stress and the crystallinity are changing. (The increase in crystallinity is due to the formation of new crystallites, considering the decrease in crystallite size during the stretching process in Figure 5.) As the number and fraction of crystallites change, the apportioning of stress to the unit volume of crystallite must be changed, and accordingly, the degree of crystal deformation should depart from the linearity with the nominal stress. (A similar opinion is also expressed by Miyamoto et al.[27] that "we should construct models including the aspects of transversal interaction among the hard domains mediated by the elasticity of soft domains", based on the results of stress−strain measurements.)

On the other hand, when we consider the deformation mechanism as a pantograph (Figure 11b), effective stress can be loaded the crystallites proportionally to the nominal one. The crystallites are assumed to exist between the frames of the pantograph. The stress may be mediated by the frames. If the nominal stress for the unit width of a row is equally transmitted to the crystallites in the row, the linear relationship between the stress and the deformation would appear. Even when the crystallinity changes with the stress (or with strain), the linearity would be retained. In the model in Figure 11b, both uniaxial stretching (in the vertical direction) and lateral compression (in the horizontal direction) are possible causes for the deformation of crystallites. It should be noted that the amorphous chains are also in the same environmentally confined space as the crystallites, and accordingly, the force must be applied in a similar way. If the coiled chains are compressed in the horizontal direction in Figure 11b, uncoiling of the chains would be difficult. This could be an additional reason why the random-coil-like state tends to be maintained, resulting in the isotropic amorphous halo in the WAXD pattern.

The role of strain-induced crystallites on the mechanical response upon stretching should be to increase the modulus and enhance the tensile strength. Because of the increase in crystallinity upon stretching, the nonlinear increase of stress would be observed in the stress−strain curve (Figure 1). However, the reinforcement effect of the crystallites may be brought out not directly from crystallites connected in series but indirectly through the surrounding network chains compressing the crystallites in the lateral directions.

Process of Contraction. When the sample was allowed to contract, the crystallites became larger (Figure 5b,d), and the orientational fluctuations decreased (Figure 6b). Because the crystallinity decreased just after the beginning of the contraction process (Figure 3), these changes indicate that the crystallites are rearranged and combined to form larger crystallites. At the same time, the stress is drastically decreased, which is consistent with the results in Figure 1. Therefore, the chains that tighten the crystallites should be relaxed and the crystallites would obtain mobility to permit the reorganization. One of the coauthors of this paper reported the increased peak intensity of the 120 reflection of the slightly retracted sample,[31] which can be attributed to the increase in crystallite size. This is because the changes in crystallite size and degree of orientation affect the width of a reflection, while the crystallinity is related to the integrated intensity of the reflection. If the averaged crystallite size becomes larger even without changing the total crystallinity, the reflection will become sharper and higher without change in integrated intensity.

Further contraction results in crystal melting due to the decrease in melting temperature, as known from eq 7, which subsequently reduces the crystallite size (Figure 5b,d). In addition, the orientational fluctuations

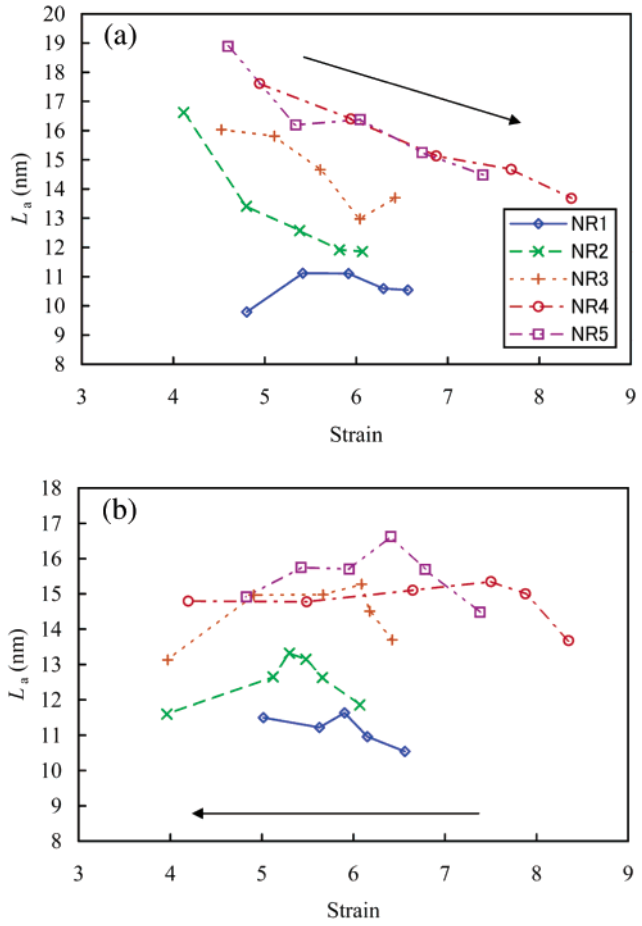

Figure 12. Variation of corrected lateral crystallite size, L_a, by using both 200 and 400 reflections: (a) during the stretching process; (b) during the retracting process.

of the crystallites increase due to the relaxation of the system, which is seen in Figure 6b.

Conclusions

By WAXD measurements of vulcanized NR samples with different cross-linking density, we obtained the following results: (1) The onset strain of crystallization upon elongation was almost independent of the network-chain density, ν. (2) Crystallinity developed with strain faster in the sample with the larger ν. (3) The values of the lateral crystallite size L_{200} and L_{120} decreased with strain in the stretching process. In the retraction process, they increased first and then decreased upon contraction due to the crystal melting. (4) The lateral crystallite size was smaller in the sample with the larger ν value. (5) The degree of orientational fluctuations of crystallites, β_{az}, was almost constant during the stretching process. When the retraction process started, first β_{az} became smaller and then increased due to crystal melting. (6) The sample with the larger ν showed the smaller β_{az}. (7) The lattice constants of the NR crystal changed almost linearly with nominal stress. The crystal lattice was elongated in the stretching direction and contracted in the lateral directions perpendicular to it. (8) The volume of the unit cell decreased almost linearly with nominal stress.

The results in (4) and (6) are related to the crystallization model that highly stretched network chains act as nuclei and lamellar crystals can be initiated from them. Coiled chains surrounding the nuclei can partake in the crystal growth.

By considering the deformation model like a pantograph, these results were consistently explained. In any cases, the results in (7) and (8) directly proved that the strain-induced crystallites are responsible for the increased modulus upon elongation.

Acknowledgment. This research was partially supported by a Grant-in-Aid for Scientific Research (B)(2), No. 15404011, from Japan Society for the Promotion of Science. The Stony Brook group thanks the financial support of National Science Foundation (DMR-0098104) and the Department of Energy (DEFG02-99ER45760).

Appendix 1

A distribution having the form of a Gaussian function

$$I(x) = h \exp[-(x - x_c)^2/(2w^2)] \tag{A1}$$

has its maximum at $x = x_c$ and the height is h. The half-width β of the distribution is obtained by solving the following equation and estimating the difference between the two solutions:

$$h/2 = h \exp[-(x - x_c)^2/(2w^2)] \tag{A2}$$

$$x = x_c \pm w\sqrt{-2 \ln(1/2)} \tag{A3}$$

Therefore

$$\beta = 2w\sqrt{-2 \ln(1/2)} \tag{A4}$$

The degree of instrumental broadening was estimated as the half-width β_{ref} from relatively sharp reflections of ZnO crystallites in the rubber samples. From the observed half-width of the rubber sample β_{obs}, the instrumental broadening was deconvoluted using the following equation:

$$\beta = \sqrt{{\beta_{obs}}^2 - {\beta_{ref}}^2} \tag{A5}$$

Appendix 2

Strictly speaking, the crystallite sizes shown in Figure 5 are smaller than the true values because the crystallites contain disorder or defects that increase the width of the reflections. The effect of disorder was excluded in the following manner. Since the value of L_{400} would be equal to L_{200} if the crystallites were perfect, or L_{400} would be smaller than L_{200} if the crystallites were disordered, by extrapolating the L_{h00} values to $h = 0$, the crystallite size in the a-direction without the effect of disorder, L_a, was estimated. Figure 12 shows the variation of L_a with strain. It is noted that the values of L_{400} and L_a had larger fluctuations due to the poorer S/N ratio for 400 reflections, especially when strain was small and crystallites were not developed. The plot of the corrected values (L_a) show essentially the same trend as in Figure 5, though some deviations from the trend are found due to the fluctuation and the values tend to be larger than those in Figure 5. For simplicity, the discussion in the main text was presented only on the basis of Figure 5.

References and Notes

(1) Mandelkern, L. *Rubber Chem. Technol.* **1993**, *66*, G61−G75.
(2) Flory, P. J. *J. Chem. Phys.* **1947**, *15*, 397−408.

(3) Holl, B.; Kilian, H. G.; Schenk, H. *Colloid Polym. Sci.* **1990**, *268*, 205−221.
(4) Conradt, R. N. J.; Heise, B.; Kilian, H. G. *Prog. Colloid Polym. Sci.* **1992**, *87*, 85−103.
(5) Luch, D.; Yeh, G. S. Y. *J. Appl. Phys.* **1972**, *43*, 4326−4338.
(6) Shimizu, T.; Tsuji, M.; Kohjiya, S. *Mater. Sci. Res. Int.* **1998**, *4*, 17−120.
(7) Tsuji, M.; Shimizu, T.; Kohjiya, S. *Polym. J.* **1999**, *31*, 784−789.
(8) Tsuji, M.; Shimizu, T.; Kohjiya, S. *Polym. J.* **2000**, *32*, 505−512.
(9) Shimizu, T.; Tosaka, M.; Tsuji, M.; Kohjiya, S. *Rubber Chem. Technol.* **2000**, *73*, 926−936.
(10) Luch, D.; Yeh, G. S. Y. *J. Macromol. Sci., Phys.* **1973**, *7*, 121−55.
(11) Mitchell, G. R. *Polymer* **1984**, *25*, 1562−1572.
(12) Murakami, S.; Senoo, K.; Toki, S.; Kohjiya, S. *Polymer* **2002**, *43*, 2117−2120.
(13) Toki, S.; Sics, I.; Ran, S.; Liu, L.; Hsiao, B. S.; Murakami, S.; Senoo, K.; Kohjiya, S. *Macromolecules* **2002**, *35*, 6578−6584.
(14) Treloar, L. R. G. In *The Physics of Rubber Elasticity*; Oxford University Press: London, 1975.
(15) Kawaguchi, A.; Murakami, S.; Katayama, K.-; Mihoichi, M.; Ohta, T. *Bull. Inst. Chem. Res., Kyoto Univ.* **1991**, *69*, 145−154.
(16) Murakami, S.; Nishikawa, Y.; Tsuji, M.; Kawaguchi, A.; Kohjiya, S.; Cakmak, M. *Polymer* **1995**, *36*, 291−297.
(17) Nishikawa, Y.; Murakami, S.; Kohjiya, S.; Kawaguchi, A. *Macromolecules* **1996**, *29*, 5558−5566.
(18) Schallamach, A. *Trans. Faraday Soc.* **1942**, *38*, 376−380.
(19) Fraser, R. D. B.; Macrae, T. P.; Miller, A.; Rowlands, R. J. *J. Appl. Crystallogr.* **1976**, *9*, 81−94.
(20) Wu, J.; Schultz, J. M.; Yeh, F.; Hsiao, B. S.; Chu, B. *Macromolecules* **2000**, *33*, 765−1777.
(21) Klug, H. P.; Alexander, L. E. In *X-ray Diffraction Procedures for Polycrystalline and Amorphous Materials*, 2nd ed.; Wiley-Interscience: New York, 1974; p 687.
(22) Nyburg, S. C. *Acta Crystallogr.* **1954**, *7*, 385−392.
(23) De Candia, F.; Romano, G.; Russo, R.; Vittoria, V. *J. Polym. Sci., Polym. Phys. Ed.* **1982**, *20*, 1525−1531.
(24) Toki, S.; Sen, T. Z.; Valladares, D.; Cakmak, M. *Proceeding of a Meeting of the Rubber Division, American Chemical Society, Providence, RI*, April 2001, pp 24−27.
(25) Valladares, D.; Toki, S.; Sen, T. Z.; Yalcin, B.; Cakmak, M. *Macromol. Symp.* **2002**, *185*, 149−166.
(26) Yamamoto, M.; White, J. L. *J. Polym. Sci., Part A-2* **1971**, *9*, 1399−1415.
(27) Miyamoto, Y.; Yamao, H.; Sekimoto, K. *Macromolecules* **2003**, *36*, 6462−6471.
(28) Amram, B.; Bokobza, L.; Queslel, L. P.; Monnerie, L. *Polymer* **1986**, *27*, 877−882.
(29) Tsuji, M.; Fujita, M.; Shimizu, T.; Kohjiya, S. *Macromolecules* **2001**, *34*, 4827−4833.
(30) Taguchi, K.; Miyamoto, Y.; Miyaji, H.; Izumi, K. *Macromolecules* **2003**, *36*, 5208−5213.
(31) Toki, S.; Fujimaki, T.; Okuyama, M. *Polymer* **2000**, *41*, 5423−5429.

MA0355608